Percolation transition at growing spatiotemporal fractal patterns in models of mesoscopic neural networks

Igor Franović* and Vladimir Miljković†
Faculty of Physics, University of Belgrade, P.O. Box 368, 11001 Belgrade, Serbia
(Received 15 November 2007; revised manuscript received 5 March 2009; published 24 June 2009)

Spike packet propagation is modeled in mesoscopic-scale networks, composed of locally and recurrently coupled neural pools, and embedded in a two-dimensional lattice. Site dynamics is governed by three key parameters—pool connectedness probability, synaptic strength (following the steady-state distribution of some realizations of spike-timing-dependent plasticity learning rule), and the neuron refractoriness. Formation of spatiotemporal patterns in our model, synfire chains, exhibits critical behavior, with the emerging percolation phase transition controlled by the probability for nonzero synaptic strength value. Applying the finite-size scaling method, we infer the critical probability dependence on synaptic strength and refractoriness and determine the effects of connection topology on the pertaining percolation clusters fractal dimensions. We find that the directed percolation and the pair contact process with diffusion constitute the relevant universality classes of phase transitions observed in a class of mesoscopic-scale network models, which may be related to recently reported data on *in vitro* cultures.

DOI: 10.1103/PhysRevE.79.061923 PACS number(s): 87.18.Sn, 68.35.Rh, 87.18.Hf

I. INTRODUCTION

The homeostatically stable state of most biological neural networks is comprised of single neurons firing asynchronously at low rates [1,2]. After receiving the input, most networks pass to coherent states, characterized by higher temporal covariance in neuron firing series [2,3]. The emerging transient synchrony in neuron firing times [4–6] provides a substrate for transmission and transformation of information [1,7] and allows the subsequent rapid relaxation of the evoked sections of the network.

Dispersed neurons, gathered in small groups by the firing synchronization, tend to be engaged in sequential activity. Groups observed at consecutive sampling intervals can be disjunctive or partially overlapping. Though the sequential dynamics usually encompasses most of the network, there may also be neurons left out of any synchronized group. By the spatial distribution of synchronously firing neurons, precisely timed firing patterns have been well documented in networks preserving the brainlike architecture (at *in vivo* recordings [7–13] and organotypic slices [14,15]) but have been recently recognized in networks with self-organized circuitry (in cultured networks [16–20]). There are two likely types of patterns to be distinguished. First, the activation sequences may consist of repeatedly reactivated neuronal groups, forming the looplike patterns. Second, in the propagative events activity spreads mainly along nonrecursive paths, allowing only occasional reverberating dynamics.

The first pattern type characterizes the distributed synchrony activity mode [21], initially observed in trained networks driven by the external stimuli [5,22]. In this mode, neural population becomes partitioned into multiple functional subassemblies, containing anatomically unconnected neurons. Complementary data seem to suggest the network activity converging onto a variety of attractors [23].

On the other hand, synchronized bursting [18,19,24,25] represents the preferred network-wide propagative dynamical mode. Revealed by multisite recordings from *in vitro* cultures plated on microelectrode arrays, additional research indicates its arousal to be often mediated by the prolonged neuron membrane potential depolarization [18]. The robustness of spontaneously generated and evoked synchronized bursts is believed to reflect the inherent functional organization in networks with quite general connection topologies [17]. The detailed structure of bursting events shows synchronized activity spreading over distinct propagation paths [26], unlike the ones in wavelike spreading phenomena. Accounting for the more complex propagation mechanisms, we introduce a model network of neural pools [27]. Pools act as functional units facilitating the spreading of synchronized spike volleys across the network. Our approach is not intended to be fully biomimetic. Its aim is to provide a trackable model capturing the gross features of the reported complex spatiotemporal patterns, which are related to the realizations of pool multiple attractor states. The research of collective phenomena in mesoscopic-scale networks [28,29] has to deal with interactions at different levels of spatiotemporal organization, including multiple recurrent connections [2,18,30]. The spatiotemporal patterns in our model may be viewed as generalizations of synfire chains [2,12,31]. With the term chain referring to temporal (causal) sequence of neuron ensemble firing, the synfire chains were proposed as modules impressing temporal directedness in networks with moderate reverberating activity [32]. Demonstrating that the synfire chain formation corresponds to a percolation phase transition enabled us to determine the arising pattern fractal properties. Though critical phenomena were observed in macroscopic neurobiological systems [33], an instance of percolation phase transition has been reported only recently [34,35].

This paper is organized as follows. The second section begins with a brief description of the possible network to-

*igor.franovic@gmail.com
†vladimir.miljkovic@ff.bg.ac.rs

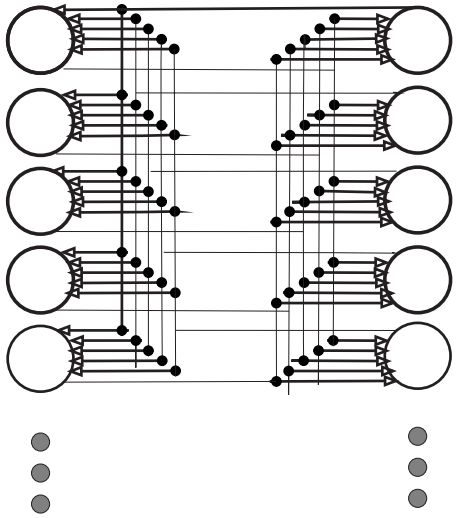

FIG. 1. Neurons are organized in homogeneous pool assemblies, represented by columns of open circles. Bold dots indicate synaptic connections. No synapses are assumed between neurons in the same pool. The approximate synchronization within the pool is provided by a common input, delivered over the divergent/convergent all-to-all type connections with neurons from the adjacent pools.

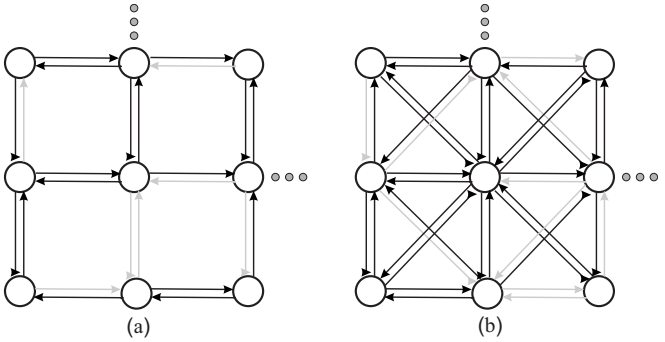

FIG. 2. The formation of synfire chains is examined for two lattice topologies, with the connection weights observing the steady-state STDP learning rule distribution. The open circles denote neural pools, and the solid lines indicate couplings between each pool and its neighbors. Black lines are assigned to bonds with nonzero synaptic weights $\omega_{ij}=\Omega$, while the gray lines represent zero weight connections. (a) Schematic of a regular lattice segment. Each pool is coupled to the sites within its von Neumann neighborhood. (b) Schematic of a lattice segment with the connection topology including the next-nearest-neighbor couplings. Bonds extend from each pool to its Moore neighborhood.

pologies sustaining the precisely timed propagation patterns. We also create a closure for pool firing activity, characterized by the generation of spike packets. The third section considers the properties of the emergent long-range order, associated with the spike packet propagation. For the incipient synfire chains, we introduce definitions and the appropriate methods to evaluate critical parameters. The fourth section outlines the results of a computer simulation, demonstrating that the synfire chain formation is accompanied by the percolation phase transition. We assess the effects of the network connection topology and the neuron dynamics parameters on the transition universality class. In the concluding section we indicate the possible mechanisms behind the observed dependence of percolation cluster fractal properties on the network parameters and argue the range of the introduced model validity and applicability.

II. MODEL

A. Network architecture

Local pool dynamics consists of spike packets, represented by the narrow distribution of neuron firing times. Since pools generally constitute functional assemblies of anatomically noncoupled and possibly spatially dispersed neurons, the needed synchronization can only be achieved by enabling the neurons to receive similar input. Such condition is met if the neurons within adjacent pools are connected in the divergent/convergent all-to-all manner, as in Fig. 1. Each pool comprises approximately 100 neurons, consistent with the experimental studies on the precisely timed recurring firing patterns [17–20,26], indicating that pools may span the range between tens and a few hundred neurons [23,36]. Though initially perceived as analogs to cortical columns *in vivo*, several reports seem to indicate the plausibility of pool notion at *in vitro* cultures (including the cultured slices) [16–20] and the organotypic slices [14,15].

Adjacent pools engaged in spike packet propagation may be associated into functional suprastructures-synfire chains. Propagation along synfire chains obviously resembles solitons and other local excitations in nonlinear extended media [27]. Synfire chains may be embedded in networks with recurrent connections, allowing reverberating activity. The extension to proper branching networks has proven difficult, since there are few conclusive data on possible coupling schemes between functional neuronal assemblies. Thus, it becomes plausible to examine the conditions for stable synfire chain formation in networks with different topologies. Specifically, we consider the two topologies characterized by interactions within the von Neumann [regular lattice, Fig. 2(a)] and Moore neighborhoods [topology with the included next-nearest-neighbor couplings, Fig. 2(b)] of each pool. Similar approach has been taken experimentally in artificially creating the so-called iteratively constructed networks of neurons [36].

The couplings are assigned weights ω_{ij}, whose lower indices i and j refer to coordinate sets of postsynaptic and presynaptic neurons, respectively. The weights may attain two possible values—zero, with probability $1-p$, and a nonzero value Ω, with probability p. The selected set can be related to some models of the spike-time-dependent plasticity (STDP), which has been suggested as the likely synaptic dynamics rule promoting persistent transmission of spike packets [1,37]. These models suggest that after elaborate training, with the STDP rules applied, synaptic weights cluster around the upper-bound nonzero value and zero [21]. The synaptic weights pertaining to forward and backward connections are identically and independently distributed. Since the characteristic time of weight change is expected to largely exceed the single spike volley duration, synaptic weights may be considered as quenched variables during the spike packet propagation.

The following two subsections outline the formalism needed to quantify the properties of spike packets. After analyzing the firing dynamics of neurons within a pool, we build the activity model appropriate for populations generating and propagating spike packets.

B. Neuron model

The neuron dynamics is set to follow the spike response model [27,38] with stochastic firing. By the model, the total membrane potential u_i at neuron i may be expressed in terms of the postsynaptic potential and the spike after-potential kernel η,

$$u_i(t) = \sum_{\langle j \rangle} \frac{\omega_{ij}}{z+1} \int_0^\infty dt' \epsilon(t') T_j(t-t') + \eta(t-\hat{t}_i). \quad (1)$$

The angled brackets $\langle\ \rangle$ denote the sum over z neighboring pools providing the input. As the model neglects the detailed form of the action potential, spike train T_j from the jth pool may be represented by the sum of Dirac δ functions $T_j = \Sigma_f \delta(t-t_j^{(f)})$, where index f stands for the respective neuron firing times. Accordingly, postsynaptic potential represents the convolution of the arriving spike trains with the neuron response kernel $\epsilon(t) = \frac{t}{\tau^2} e^{-t/\tau} \Theta(t)$, where τ refers to the membrane time constant. Since the generation of the next spike is assumed to depend only on time $\hat{t}_i$ of the last spike in the prior firing sequence, the neuron spiking dynamics can be described by an input-dependent renewal process [27,38,39].

Equation (1) may further be accommodated to explicitly relate the neuron membrane potential and the neighboring pool firing activity. Allowing that the number of neurons N within presynaptic pools is sufficient for the law of large numbers to apply, the pool activation $A(t)$ is introduced as the fraction of neurons emitting action potential in the small time interval Δt,

$$A(t) = \lim_{\Delta t \to 0} \frac{1}{\Delta t} \frac{n_{act}(t, t+\Delta t)}{N} = \frac{1}{N} \sum_{l=1}^{N} \sum_f \delta(t - t_l^{(f)}). \quad (2)$$

We assign $n_{act}(t, t+\Delta t)$ to the number of active neurons within the $[t, t+\Delta t]$ interval. Applying Eq. (2), the membrane potential on neuron i in the given pool k (the index k refers to the pool coordinate set) relates through a recurrent formula to the input activation from z neighboring pools,

$$u_i^k(t) = \sum_{\langle j \rangle} \frac{\omega_{ij}}{z+1} \int_0^\infty \epsilon(t') A_j(t-t') dt' + \eta(t-\hat{t}_i). \quad (3)$$

With A_j we denote the activation on the jth pool adjacent to pool k.

The spike after-potential kernel, generally comprising the membrane reset potential and the refractory period, is introduced by the absolute refractoriness approximation

$$\eta(t-\hat{t}) = \begin{cases} -\infty, & 0 \le t-\hat{t} \le \mu \\ 0, & t-\hat{t} > \mu, \end{cases} \quad (4)$$

which precludes the neurons from firing any additional spikes during the absolute refractory period μ.

Values of τ and μ may further be specified by taking into account that the neurons at pools engaged in spike packet propagation are not expected to show large amplitude fluctuations of the membrane potential. The neurobiological data suggest that the highly synchronized input these neurons receive consists predominantly of the excitatory postsynaptic potentials ("synaptic bombardment" [26,40]), keeping the membrane potential in the high-conductance "up" (depolarized) state [18,31,41]. Such neuron states are characterized by reduced membrane time constants, decreasing from approximately 10 ms to very low values (approximately 2 ms [42,43]). Accordingly, the membrane time constant in our simulation is set to 2 ms. While the small membrane time constants τ cause the neurons to fire only if a significant number of synchronized presynaptic spikes arrives at the neuron [27], the comparable or comparably larger absolute refractoriness values μ additionally ensure that neuron firing rates are not enlarged excessively. (Further on, it is convenient to express μ in units of τ.) At the ensemble level, the μ value is chosen adequately to prevent receiving pool feedback from eliciting additional spikes at the source pools during the input volleys.

The stochasticity in the neuron firing dynamics may be related to the observed potential values by the hazard function $f(u(t))$ (instantaneous or conditional probability density of firing) [27,44], which is applied to model the escape noise. In the absence of nonlinear transfer function or firing threshold, the single hazard function has to be chosen properly to account for the possible noise effects (membrane potential fluctuations, synaptic, and ion-channel noise). Consistent with the membrane potential states, a simple yet sufficient choice for the hazard function may be the step-linear function

$$f(u) = \begin{cases} u, & u \ge 0 \\ 0, & u < 0, \end{cases} \quad (5)$$

since the firing probability density is known to follow the membrane potential growth monotonously if confined to neurons that are about to emit action potential [27]. The provided neuron model details enable building the network dynamics in a self-consistent manner; the incoming synchronized local activity influences the state variables and the hazard function of the receiving neuron, which in turn, takes part in the propagation of synchronized activity through the network.

C. Population dynamics

To determine the properties of spike packet propagation, it is necessary to relate the population dynamics at each pool with the activities on pools delivering the input. A closure for the population activity $A(t)$ (the pool index on the activation variable is dropped to keep the notation simple) is created by applying the arguments of the ergodic theorem. By the theorem [44], the firing probability density $\hat{f}(t)$ for the single neuron to discharge at t is evaluated as the normalized number of spikes observed in population during the interval $[t, t+dt]$, divided by the interval length dt, which is of the order of τ. Thus, according to definition (2), the pool aver-

aged activity $A(t)$ at moment t can be taken as equal to the firing probability density $\hat{f}(t)$ of the single neuron. If $\hat{t}$ is the last firing time prior to t, the probability density $\hat{f}(t)$ to generate the next spike at t may generally be estimated as a product of the survival probability function [27,38,44,45], $S(t|\hat{t})$, and the conditional probability to discharge within the following small interval $[t,t+dt]$. The conditional probability is, by definition, the hazard function $f(u'(t))$, where $u'(t)$ stands for postsynaptic potential [first member on the right side of Eq. (1)] [27,38]. Thus, the firing probability density $\hat{f}(t)$ is given by $\hat{f}(t)=f(u'(t))S(t|\hat{t})$.

In order to consistently relate neuron dynamics with the dynamics of homogeneous neural population (pool), certain criteria need to be met. By construction, all neurons within a pool have the same postsynaptic membrane potential $u'(t)$. The stronger criterion concerns the small value of membrane time constant τ, which causes the neurons to fire at low rates. The latter affects the survival probability function in such a way that function $S(t|\hat{t})$ is weakly time dependent. For the renewal processes [27,38,39,44,45] referred to in Sec. II B, $S(t|\hat{t})$ is given as a homogeneous function of time, $S(t|\hat{t})=\exp\{-\int_{\hat{t}}^{t} f[u'(t')+\eta(t'-\hat{t})]dt'\}$. The $S(t|\hat{t})$ homogeneity and weak time dependence suggest that one can introduce the new function $\tilde{S}(t|\hat{t})$, so that relation $\tilde{S}(t|\hat{t})\approx S(t|\hat{t})$ holds,

$$\tilde{S}(t|\hat{t})=\exp\left\{-\int_{0}^{t} f[u'(t')+\eta(t'-\hat{t})]dt'\right\}. \tag{6}$$

We note that $\tilde{S}(t|\hat{t})$ represents an auxiliary function defined for numerical purposes. The proposed ansatz on $\tilde{S}(t|\hat{t})$ is an immediate consequence of the considered model conditions (equality of postsynaptic membrane potentials within a pool and small membrane time constants) and the ensuing ergodicity. We argue that each neuron can be assigned with unique $\hat{t}$ value, consistent with the assumption that neuron can fire once or not at all during a single spike packet. This is possible if the spike packet width is comparable to μ, which makes it highly unlikely for the neuron to fire twice or more within a packet. Based on the equality of $\hat{f}(t)$ and $A(t)$ (ergodicity), using the ansatz on $\tilde{S}(t|\hat{t})$, the population activation becomes

$$A(t)=f(u'(t))\tilde{S}(t|\hat{t}), \tag{7}$$

where the variable on the left characterizes the pool and the expression on the right relates to the representative neuron from that pool. While the first factor on the right takes the same value for all the neurons within the pool, the other factor depends on $\hat{t}$ of the representative neuron. By the choice of representative neuron, the firing time $\hat{t}$ can belong to either $[0,t-\mu]$ or $[t-\mu,t]$ interval. Thus the expression on $\tilde{S}(t|\hat{t})$ can conveniently be rewritten as

$$\tilde{S}(t|\hat{t})=\exp\left\{-\int_{0}^{t-\mu} f[u'(t')+\eta(t'-\hat{t})]dt'\right\}\times\exp\left\{-\int_{t-\mu}^{t} f[u'(t')+\eta(t'-\hat{t})]dt'\right\}. \tag{8}$$

As a consequence of ergodicity, the second factor may be interpreted as the fraction of neurons that did not fire in the $[t-\mu,t]$ interval. We substitute this factor by the exact fraction $(1-\int_{t-\mu}^{t}A(t')dt')$ of neurons remaining inactive, irrespective of whether $\hat{t}\in[t-\mu,t]$ or $\hat{t}\notin[t-\mu,t]$. By analogy, the first factor in Eq. (8) can be analyzed for the cases when $\hat{t}\in[0,t-\mu]$ or $\hat{t}\notin[0,t-\mu]$. If $\hat{t}\notin[0,t-\mu]$, the first factor becomes $\exp[-\int_{0}^{t-\mu}f(u'(t'))dt']$. In the case $\hat{t}\in[0,t-\mu]$, due to refractoriness, the hazard function by definition (5) becomes 0 in the $[\hat{t},\hat{t}+\mu]$ interval. If the duration of propagation process $t\gg\mu$, the effect of η kernel can be neglected.

By the given analysis on $\tilde{S}(t|\hat{t})$, we arrive at the expression

$$\tilde{S}(t|\hat{t})=\exp\left[-\int_{0}^{t-\mu} f(u'(t'))dt'\right]\left[1-\int_{t-\mu}^{t} A(t')dt'\right], \tag{9}$$

which holds for population dynamics, irrespective of the choice of the representative neuron. Inserting Eq. (9) into Eq. (7), the expression for the averaged population activity at t becomes

$$A(t)=f(u'(t))\exp\left[-\int_{0}^{t-\mu} f(u'(t'))dt'\right]\left[1-\int_{t-\mu}^{t} A(t')dt'\right]. \tag{10}$$

The preceding equation, together with Eq. (3), comprises a two-step iterative equation for population dynamics, as the dependence on activation from pools delivering the input is given through membrane potential. The approximate formula (10) is comparable to the Wilson-Cowan equation [27,46] and the population activity equation presented in [38]. The differences among them reflect the respective conditions under which the populations receive and generate neuron activity.

The proposed population activity model should ensure that pool dynamics converges to attractors, with characteristics influenced by the network topology. When studying spike packet propagation, local pool states are commonly described by the zeroth and second moments of activation distribution [7,22,38], corresponding to integral activation $\bar{A}$ and activation dispersion, respectively. Here we analyze the pattern formation by observing the spatial sequences of pool integral activation values $\bar{A}_j$ (j refers to the set of pool coordinates) through consecutive network layers. The propagation of spike packets is supposed to satisfy three conditions: stability, reproducibility, and long-time duration [2]. Thus, with the large enough external input provided at the seed pool, long-range order of pool integral activation is expected to appear.

III. CRITICAL PARAMETERS

A. Long-range order

A two-dimensional network is introduced with a single high-activation spike packet at the seed pool to enable the neuron activity spreading across the system. Clustering of pool integral activation values $\bar{A}_j$ is observed in a three-dimensional parameter space. With varying values of synaptic strength Ω, pool connectedness probability p, and refractoriness μ, we find the pool ensemble dissolving into classes (subgroups), with, up to the computational bin, an identical value of integral activation. The proper bin value is determined in a self-consistent manner by enhancing its value until the number of distinct classes ceases to reduce. Neighboring pools belonging to the same class comprise clusters. For the fixed refractoriness and weight values, clusters spanning the whole network appear only after a certain threshold pool connectedness probability $p_c(\Omega,\mu)$ is surpassed. Though at first this property may seem to relate to bond percolation, the model is clearly more complex, since the formation of percolation clusters is assessed by the spatial distribution of the continuous site variable values. The other less obvious difference to genuine bond, site, and bond-site percolation models comes from the fact that variable p, which refers to the presence (or absence) of synaptic connections, merely indirectly affects the formation of pool clusters, following Eq. (10).

Relative to the critical threshold $p_c(\Omega,\mu)$, we observe three dynamical modes, which occupy distinct subspaces of the parameter space. First, the system is in the *subcritical state* for $p<p_c$ when the pools belong to many different classes and form only small clusters. The system is in the *critical state* for $p=p_c$ when the incipient percolation cluster appears. Finally, in the *supercritical state* $p>p_c$, many of the pools pertain to the same class or even the same cluster (Fig. 3). We represent the pool clustering at three characteristic states by introducing histograms of fraction of pool pairs $P_{\Delta\bar{A}}$ with the exact integral activation difference $\Delta\bar{A}$, expressed in units of activation bin. Fractions of pool pairs are normalized over the total number of pool pairs in the network. We note that the integral activation values on pools constituting percolation clusters significantly differ from the one on the seed pool, implying that the resulting dynamics mainly depends on the functional organizing of the network.

B. Finite-size scaling

We evaluate the critical probabilities p_c and the critical exponent ratios $\frac{\beta}{\nu_\perp}$ to characterize the critical behavior of the observed percolation phase transition. The order-parameter is defined as

$$m = \left| \rho - \frac{1}{2} \right|, \tag{11}$$

with ρ being the normalized number of pools belonging to the percolation cluster. The subtraction of $\frac{1}{2}$ is introduced to account for the transition from the site occupancy to Ising-like variables, enabling the proper definition of the magnetizationlike order parameter. With the quenched character of the pool connectedness variables, the actual order-parameter values are obtained through averaging over many copies (replicas) of the system, maintaining the identical input and coupling parameters. Since the simulation of large networks would entail excessive computational resources, we apply the finite-size scaling method to determine the critical probability. In addition, the evaluation of the critical exponent ratio $\frac{\beta}{\nu_\perp}$ is required when calculating the percolation cluster fractal dimension.

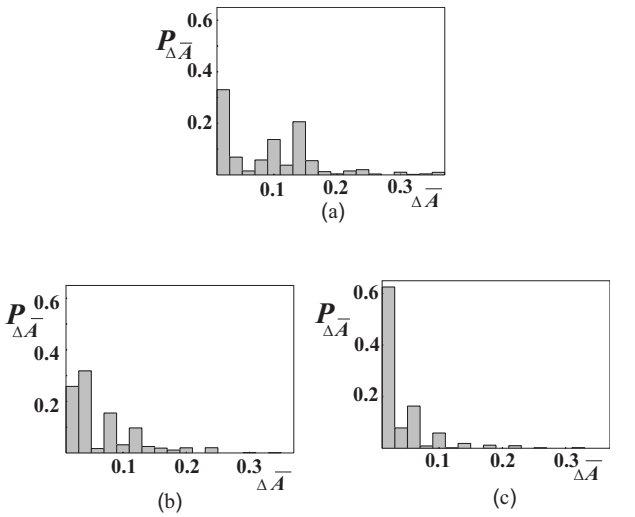

FIG. 3. Distribution of integral activation differences $P_{\Delta\bar{A}}$ on pairs of pools (a) below, (b) in the vicinity, and (c) above the critical probability p_c. With increasing probability values, pools are progressively clustered in growing classes. The example is provided for the regular lattice topology at synaptic weight $\Omega=0.4$ and $\mu=0$. Integral activation differences $\Delta\bar{A}$ are expressed in the activation bin units.

The critical probability value may be obtained by utilizing the appropriate finite-size scaling features of the Binder cumulants [47]. In the percolation threshold vicinity, for the given synaptic weight and refractoriness values, Binder cumulants (i.e., reduced fourth-order cumulants) are calculated according to [47–49]

$$U_L(p) = 3 - \frac{\langle m^4(p)\rangle}{\langle m^2(p)\rangle^2}, \tag{12}$$

where $\langle m^4(p)\rangle$ and $\langle m^2(p)\rangle$ denote the fourth and the second moments of the order-parameter distribution. The lower index L indicates the Binder cumulant general dependence on lattice size. On the other hand, the Binder cumulant finite-size scaling relation [49]

$$U_L(p) = \hat{U}[(p-p_c)L^{1/\nu_\perp}] \tag{13}$$

establishes its value to be size independent precisely at the critical probability p_c. Accordingly, the Binder cumulant curves, sampled in the percolation threshold vicinity for diverse lattice sizes, are expected to exhibit a common intersection point.

By plotting the Binder cumulants $U_L(p)$ vs p, we locate the intersection point and determine its probability coordinate. This coordinate value should represent the best estimate for the critical probability p_c [50]. The evaluated p_c values may provide information on the connectivity degree necessary for the network to sustain synfire chains.

The synfire chain fractal dimension D is calculated according to the well-established hyperscaling relation [48]

$$d - D = \frac{\beta}{\nu_\perp}, \tag{14}$$

where d represents the lattice dimensionality. The required critical exponent ratio may be obtained by applying the finite-size scaling relation of the order parameter [48],

$$m_L(p) = L^{-\beta/\nu_\perp} F_\mu[(p - p_c)L^{1/\nu_\perp}], \tag{15}$$

which at p_c leads to

$$m_L(p_c) \sim L^{-\beta/\nu_\perp}. \tag{16}$$

Consequently, if a log-log plot of the order-parameter dependence on lattice sizes is made for the previously determined critical probability, the line slope should represent a good estimate for the $\beta/\nu_\perp$ value. With the critical exponent ratios provided for, it is possible to calculate the percolation cluster fractal dimensions for the varying weight and refractoriness values. The presented methods are applied to determine the critical behavior of synfire chain formation on square-lattice networks with pools connected to their von Neumann or Moore neighborhoods.

IV. RESULTS

A. Regular lattice

Applying the methods explained in Sec. III, we obtain the critical parameters of the percolation phase transition emerging on a network with the regular lattice topology. While the considered set of synaptic weights Ω is drawn from the neurobiologically plausible range, the refractoriness μ attains values concurring with the general requirements for the model consistency (see Sec. II B). For each pair of weight and refractoriness values, we evaluate the critical probability by drawing a graph of the Binder cumulant curves at growing lattice sizes (see Fig. 4). We note that the intersection points of successive curves appear to drift slightly toward higher probabilities, which has earlier been observed in the numerical evaluation of percolation thresholds [50]. This type of systematic uncertainty here seems to be related with the inability to obtain Binder cumulants as genuine self-averaging quantities, since the number of simulated system replicas is limited.

The estimated results for the critical probability are presented in the weight-probability parameter space, with the critical probabilities at fixed refractoriness values comprising critical lines (Fig. 5). At fixed μ, the monotonous decay of p_c value is likely related to slow increase in the integral activation values of the percolation cluster. As the family of critical lines shows, the increase in refractoriness μ while keeping the constant weight Ω decreases the critical probability p_c.

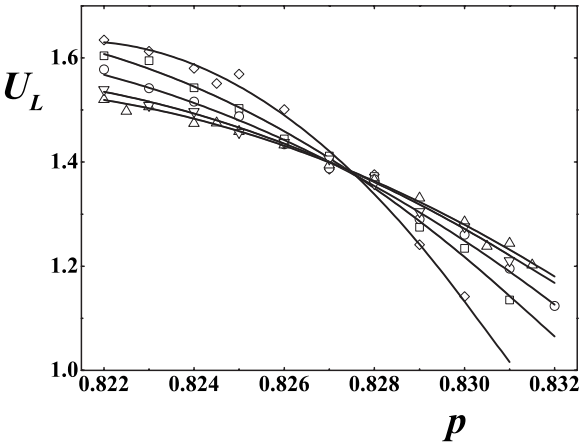

FIG. 4. Determining the critical probability value by the Binder cumulant method for $(\Omega,\mu)=(0.7,4)$. The plotted curves represent Binder cumulants U_L with respect to probability p at several lattice sizes: 32×32 (△), 40×40 (▽), 48×48 (○), 56×56 (□), and 64×64 (◇). The shape of the curves was obtained by interpolating in the second-order approximation. The fluctuation of the Binder cumulant value at each point depends on lattice size. With an increasing number of trials, fluctuations decrease more slowly at smaller than at larger lattice sizes. For instance, to stabilize the shape of curve for lattice dimension $L=32$, we needed to perform over 300 trials, while for $L=64$ it took us about 100 trials. The curves are expected to intersect at a single point, with its probability coordinate being the estimate for the critical probability value p_c.

This indicates that synfire chains could emerge in less connected networks. Applying the finite-size scaling relation (16), we estimate the critical exponent ratio $\beta/\nu_\perp$ by determining the slope of the double-logarithmic plot of the order parameter m vs system size L for the previously evaluated set

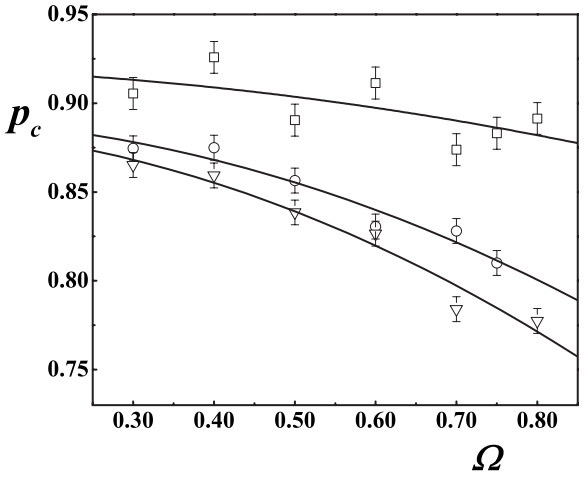

FIG. 5. Family of critical lines for refractoriness taking values $\mu=0$ (□), 4 (○), and 8 (▽). The results are presented in the weight-probability parameter space, with the critical probabilities p_c for fixed refractoriness values comprising critical lines. The network is found in a subcritical state for $p<p_c$ and each refractoriness value. The system reaches criticality at $p=p_c$, while for $p>p_c$ the neural network pertains to supercritical state.

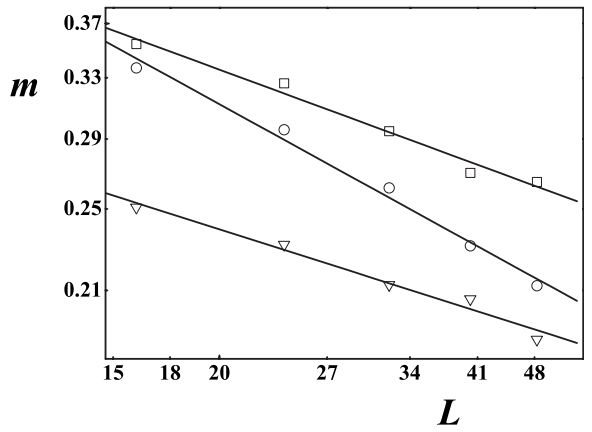

FIG. 6. Calculating $\beta/\nu_\perp$ ratios for the regular lattice topology. Log-log plots of the order-parameter values m vs system size L (where L equals the number of pools along a single side of the square lattice) are obtained at the critical probabilities p_c. The line slopes represent an estimate for the critical exponent ratios $\beta/\nu_\perp$. The particular plots, observed for the fixed weight value $\Omega=0.3$ and $\mu=0$ (○), 4 (□), and 8 (▽) illustrate the critical exponent ratio dependence on refractoriness.

of p_c values. We bring an instance of these graphs at the fixed weight value to illustrate the ratio dependence on refractoriness (Fig. 6).

The ensuing synfire chain fractal dimensions, calculated according to the hyperscaling relation (16), are presented in Table I. The results obviously cluster in two classes, corresponding to zero and nonzero refractoriness values. We note that fractal dimensions above the zero refractoriness value are higher than at $\mu=0$, suggesting that the percolation clusters at zero refractoriness are more compact than for higher refractoriness values. The fractal dimensions at $\mu>0$ may be considered equal within the numerical error.

It is likely that the percolation cluster compactness is affected by two complementary influences: "spatial averaging" (based on the neural pool connectivity degree) and single pool activation memory effect (due to temporal autocorrelation). For the regular lattice topology, the spatial-averaging effect is limited due to the low connectivity degree z. Turning on the memory effect, with nonzero refractoriness values, it is more likely for local integral activations to become trapped in mutually isolated states, characterized by a wide range of values. With the small spatial averaging, even the low refractoriness values are sufficient to induce more inhomogeneous (dispersed) percolation clusters, with larger fractal dimensions. Thus, the increased refractoriness values cannot be expected to significantly change the number of diverse pool states. Considering the significant difference in fractal dimensions at and above $\mu=0$, we assume that the percolation phase transitions at zero refractoriness belong to the universality class other than the nonzero refractoriness phase transitions. We take interest in transitions at higher μ values, since the results at zero refractoriness may not be of biological relevance. Judging by the average $\beta/\nu_\perp$ values at $\mu=4$ [0.26(6)] and $\mu=8$ [0.25(5)], we believe that these phase transitions belong to the directed percolation (DP) universality class [51–53]. Since the obtained critical exponent ratios are similar for $\mu>0$, the crossover to DP probably arises at small μ values, possibly even at $\mu=0$.

TABLE I. Hausdorff-Besicovitch fractal dimensions of percolation clusters for the regular lattice topology. The results assemble in two classes, corresponding to zero and nonzero refractoriness values, with the generic transitions at nonzero refractoriness pertaining to the DP universality class.

μ	Synaptic weight Ω			
	0.3	0.5	0.7	0.8
0	1.55(5)	1.55(5)	1.55(5)	1.57(5)
1	1.78(5)	1.74(5)	1.76(5)	1.79(5)
4	1.72(5)	1.77(5)	1.74(5)	1.66(6)
8	1.75(5)	1.73(5)	1.77(5)	1.74(5)

The recent experimental study [54] concerning the propagation of synchronized spike activity in a mesoscopic cultured network revealed the dynamics governed by the avalanche process. Therein, action potentials generated within a specified time window on neuron aggregates around the electrode comprise peaks of local-field potential. Such peaks are arranged into clusterlike suprastructures by implementing the method comparable to functional pooling. In spite of differences in defining the order parameter (while we gather all the spikes within medium size time interval, the authors of [54] observed the number of local-field potential peaks in a small time interval), the critical exponents obtained in [54] may be interpreted as pertinent to the DP universality class [55].

B. Topology with the included next-nearest-neighbor coupling

We examine the formation of synfire chains on a square lattice with the included next-nearest-neighbor couplings to establish how the connectedness degree influences the universality class of the observed phase transition. The critical parameters are estimated for the same set of weight and refractoriness values as on the regular lattice.

The obtained critical probabilities, presented in the weight-probability plane (see Fig. 7), exhibit the behavior significantly different than the one observed for the regular lattice (Fig. 5). The p_c values at fixed μ vary nonmonotonously when increasing Ω, with the nonzero refractoriness graphs displaying relative peaks within bounded weight intervals.

The observed nonmonotonicity may be related to the emerging competition between the leading and bulk clusters. The leading cluster properties (activation and spreading) are seed dominated, with its spreading mainly along the preferent spatial direction (which may dynamically be interpreted as the temporal axis). Complementarily, the bulk clusters appear as a result of the collective network dynamics (pool cross correlation) and encompass the nodes outside the preferent spreading direction. Due to a higher connectivity at $z=8$, the bulk clusters reduce in numbers but attain more lattice sites. Thus, in contrast to the $z=4$ case, the bulk clusters may be expected to percolate. On the other hand, the leading

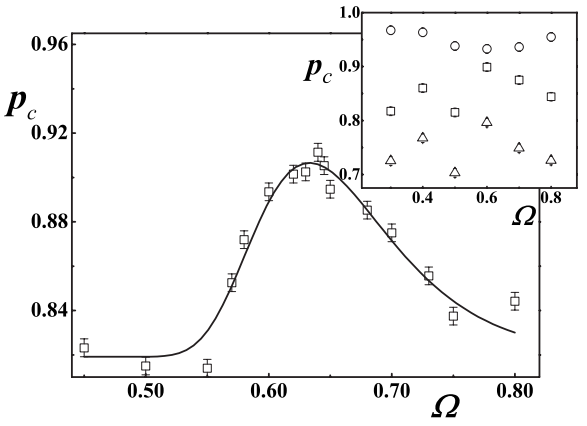

FIG. 7. Critical probability p_c dependence on weight Ω. The inset displays critical probabilities for a set of refractoriness values: $\mu=0$ (○), 4 (□), and 8 (▽). The main frame represents the enlarged peak segment of critical probability dependence on weight at $\mu=4$. The network is in subcritical state for $p<p_c(\mu)$, while the system at $p=p_c(\mu)$ and for $p>p_c(\mu)$ pertains to critical and supercritical states, respectively.

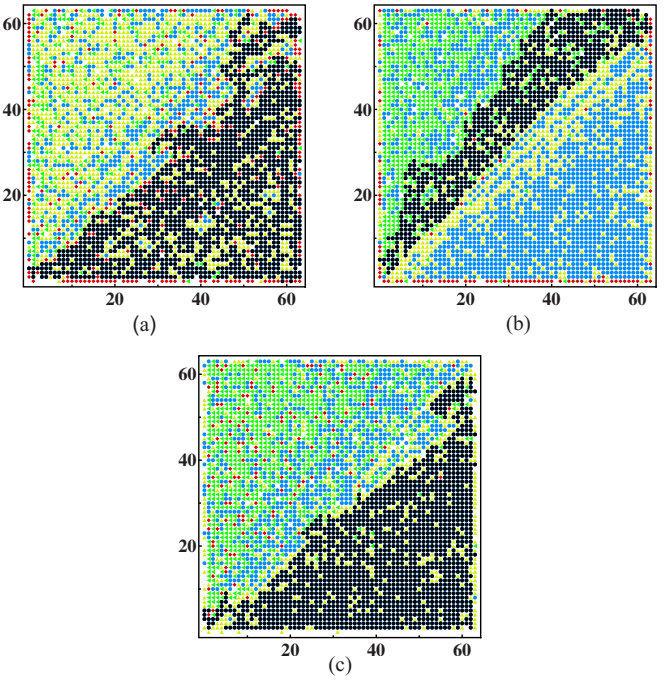

FIG. 8. (Color online) Percolation cluster snapshots at three Ω values, demonstrating the takeover scenario between the leading and the bulk cluster. The seed pool is taken to be at the origin of the graph. Pools belonging to the four main integral activation classes are represented by colored (grayscaled) symbols: black and blue (dark gray) circles are assigned to pools comprising the class of percolation cluster, with the black circles singling out the members of percolation clusters. Yellow (light gray) up triangles, green (medium gray) left triangles and red (darkest gray) diamonds are used to denote pools from the three other integral activation classes. (a) At $\Omega=0.55$, the leading cluster is observed to percolate. The percolation cluster structure is inhomogeneous, interspersed with cavities formed mainly of pools outside its activation class. (b) At $\Omega=0.62$, the bulk cluster is found as percolative. (c) At $\Omega=0.75$, the leading cluster regains the role of percolation cluster, with a more homogeneous structure (i.e., with less cavities) than at $\Omega=0.55$.

cluster spreading is weight dependent. At low Ω, the leading cluster is observed to percolate [see Fig. 8(a)]. At a certain interval of moderate Ω values we find the role of percolation cluster being taken by the bulk cluster [Fig. 8(b)]. Beyond this interval, with Ω sufficiently increased, the prevalence of the leading cluster is regained [Fig. 8(c)].

The takeover scenario consists of two parts. In the first part, the bulk cluster gains strength, which in most cases leaves the leading cluster without important links. Accordingly, the number of nonzero synaptic weights rises to enable the percolation of the bulk cluster [see Fig. 8(b)]. This accounts for the peak of critical probability in Fig. 7.

While the first part of the scenario corresponds to the rising part of the peak in Fig. 7, the second part coincides with the Ω interval beyond the peak. At Ω of roughly about 0.62, the leading cluster becomes percolative again. With the weight increase, the cross correlations between pools become more pronounced. Then the smaller number of nonzero synaptic weights is sufficient for the percolation cluster formation, allowing the lower p_c values. We expect that the critical probability peak would become sharper if the lattice dimensions were increased.

By Eq. (16), the critical exponent ratio $\beta/\nu_\perp$ may be evaluated by plotting the order-parameter dependence on lattice size at critical probability p_c. An instance of graphs at fixed Ω for the set of μ values shows how $\beta/\nu_\perp$ changes with refractoriness (Fig. 9).

The percolation cluster fractal dimensions, determined by hyperscaling relation (16), are brought in Table II. We note that the fractal dimensions for higher refractoriness values are significantly lower than for smaller ones, implying that clusters become more compact at higher μ.

The competition of the influences identified in Sec. IV A is also expected to govern the fractality of percolation clusters for the topology including the next-nearest-neighbor couplings. In this more connected network, the temporal autocorrelation cannot induce the isolated trapped local states as easily as for $z=4$. Following on that, we note that refractoriness affects the emerging of percolation clusters nontrivially. For small μ, the temporal autocorrelation at single pools is low, which leaves the formation of percolation clusters to the spatial component of the dynamics determined by Eq. (10). At moderate values of μ, which keep the temporal autocorrelation sufficiently low to prevent the "trapping" of local states, the cross correlation between the neighboring sites increases significantly. Specifically, the temporal autocorrelation is brought to the level of collective phenomenon, which enables the formation of more compact percolation clusters with low fractal dimensions. Further enhancing μ, the autocorrelation at single pools appears sufficient to overcome the influence of the spatial connectedness, leading to a slight increase in fractal dimensions.

We note that the difference in the average critical exponent ratios $\beta/\nu_\perp$ calculated for $\mu=4$ and $\mu=8$ slightly surpasses the 10% margin usually accepted in classifying phase transitions to the same universality class. Even so, we believe that most of the nonzero refractoriness phase transitions

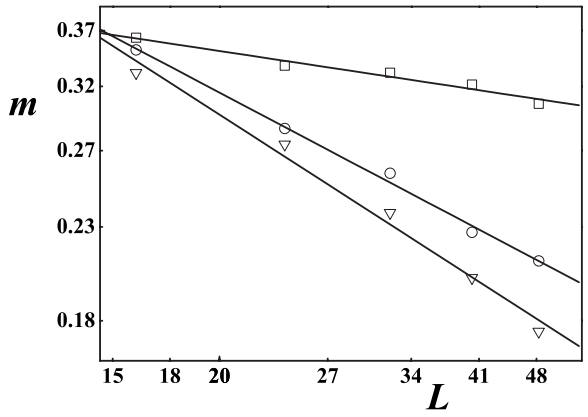

FIG. 9. Calculating the $\beta/\nu_\perp$ critical exponent ratio for the lattice topology including the next-nearest-neighbor couplings. Log-log plots of the order-parameter values m vs system size L, obtained at critical probabilities, are presented for the synaptic weight $\Omega=0.4$ and refractoriness taking values $\mu=0$ (□), 4 (○), and 8 (▽). Unlike the regular lattice topology, the plots for $\mu=4$ and $\mu=8$ exhibit different slopes, indicating the distinct $\beta/\nu_\perp$ critical exponent ratio values.

may still belong to the unique pair contact process with diffusion (PCPD) [56–59] universality class or the generalized PCPD (GPCPD) [60].

The issue of establishing PCPD as the novel nonequilibrium phase-transition universality class has proven controversial, with some authors claiming that the simulated lattice systems with the PCPD reaction-diffusion dynamics exhibit long transients to DP [57]. Based on the confirmed nontriviality of the supposed PCPD to DP crossover [61] and the several carefully ran simulations examining different PCPD realizations [56,59,62,63], the prevailing belief is that the PCPD truly represents the separate universality class. One of the possible means to distinguish between these two universality classes has been proposed in [60], where the authors argued that the long-term memory effects could represent the key perturbation from DP to PCPD. Within the GPCPD model, there exists a continuous transition from the DP to PCPD class, controlled by the "memory parameter" r, which is equal to the immediate survival probability of the particle pair, created by recombination, i.e., solitary particle collision. Thus, the DP and the PCPD universality classes correspond to the cases of complete absence ($r=0$) and the maximum memory effects ($r=1$), respectively. We believe that the mechanism similar to the described "long-term memory" may be present in our model, with the next-nearest-neighbor interaction facilitating stronger feedback, which enables the neuronal activity from certain lattice sites, acting as secondary sources, to travel backward and reactivate relatively distant pools along and near the previously covered propagation path. This effect may be compared to the dynamics of PCPD; the solitary particles are only created as residue from the branching process but may spend relatively long times in diffusion before recombining into a particle pair.

The issue of the PCPD critical exponent values has not yet been settled, with the obstacles due to the failure of the master-equation field theory [64] and the relative complexity of any supplemental models [65]. Though some papers establish the dependence of $\beta/\nu_\perp$ ratios on the diffusion constant [58,66] (providing variation in the [0.41,0.50] range), several authors reported the universality of critical exponents, with growing corrections to scaling as the diffusion constant is increased [56,59,63,65]. On the other hand, the GPCPD model predicts continuous variation in the critical exponent ratios, which encompass values between 0.28 and 0.5 within the entire memory parameter r interval [60]. The diffusion constant in PCPD and the memory parameter in GPCPD are observed to play the reversed roles with respect to the critical exponent change. The results for the refractoriness-controlled $\beta/\nu_\perp$ ratio change we report [0.56(6) at $\mu=4$ and 0.49(6) at $\mu=8$] appear to be consistent with the GPCPD model [60] but also concur with some authors who obtained the nonuniversal critical exponents for the PCPD universality class [58,66]. According to the obtained critical exponent values, the universality classes of the transitions at $\mu=4$ and $\mu=8$ seem to differ from the ones at $\mu=0$, indicating a possible crossover.

In addition to comments following Fig. 7, we provide further insight to nonmonotonicity of critical probability in view of the considered universality classes. By values of $\beta/\nu_\perp$, we note that phase transitions within the weight intervals corresponding to the rising part of the peak in Fig. 7 may belong to the dynamic isotropic percolation (DIP) [53] universality class. The crossover is influenced by the changes in the integral activation of percolation cluster. Namely, the network state may be viewed through spatial distribution of pools, whose integral activation assumes the value corresponding to one of the coexisting fixed points. Within the crossover scenario, the integral activation of percolation cluster switches between different fixed points, which disturbs the observed state structure generic for the PCPD transitions. An instance of the described mechanism, provided

TABLE II. Percolation cluster fractal dimensions for networks with pools interacting within their Moore neighborhoods. The results obtained at $\mu=4$ and $\mu=8$ indicate that the transitions, emerging for the parameter values meeting the terms of biological plausibility, predominantly pertain to the PCPD universality class.

μ	Synaptic Weight Ω					
	0.3	0.4	0.5	0.6	0.7	0.8
0	1.85(4)	1.86(4)	1.85(4)	1.87 (4)	1.84(4)	1.93(5)
1	1.82(4)	1.85(4)	1.79(6)	1.83(4)	1.83(4)	1.81(4)
4	1.42(4)	1.44(4)	1.42(4)	1.90 (4)	1.41(4)	1.46(4)
8	1.52(4)	1.53(4)	1.53(4)	1.90 (4)	1.47(4)	1.56(4)

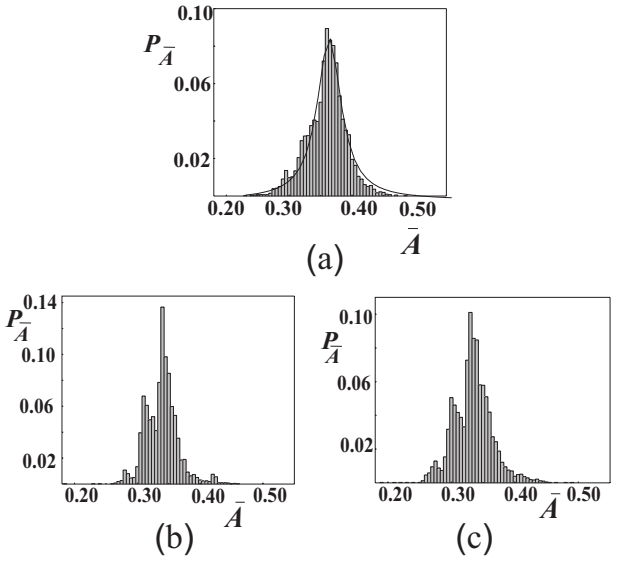

FIG. 10. Pool integral activation distribution $P_{\bar{A}}$ before, at, and beyond the peak of critical probability dependence on weight for $\mu=4$. While the distribution at $\Omega=0.55$ may be fitted to a Lorentzian-like form, the distributions for $\Omega=0.64$ and $\Omega=0.75$ display a visible secondary peak. As the former distribution accompanies the DIP universality class phase transition, the two latter distributions correspond to the PCPD universality class. Just beyond the maximum critical probability, the primary peak is at its highest value relative to the secondary peak, while their ratio gradually becomes smaller as Ω increases.

for $\mu=4$, may be unraveled by observing the weight increase induced changes in the pool integral activation distribution $P_{\bar{A}}$, obtained for very low bin value. With the smaller peak of the distribution corresponding to the percolation cluster, the remaining distribution part has to represent the absorbing states. Just below the weight interval coinciding with the rising of the critical probability peak, and for the Ω values beyond the peak [Figs. 10(b) and 10(c)], the pool integral activation distribution exhibits a visible secondary peak. On the other hand, for the Ω interval corresponding to the critical probability peak rising [Fig. 10(a)], the pool integral activation distribution is smeared out, displaying no secondary peak. The ensuing absorbing state structure remains solely for the brief weight interval featuring DIP phase transitions, with the characteristic PCPD structure recovered beyond that interval. The transitions pertaining to PCPD may be related to the average path, covered by the recurrent activity, being larger than the lattice coupling range. In the narrow Ω interval characterized by DIP transitions, the average recurrent activity path should become comparable to the interaction range, making the system state vulnerable to small perturbations and therefore spatially more homogeneous.

The critical exponent value $\beta\sim0.65$ (for both the excitatory and mixed excitatory-inhibitory populations), reported in a recent paper on percolation in cultured networks [34], seems to be consistent with the results for PCPD [53,56,58] and GPCPD universality classes [60]. That paper considers critical branching on directed random graph as the leading mechanism of synchronized activity propagation. The actual mechanism is possibly more complex, including sufficient recurrent loops that facilitate the memory effects, known to advance the PCPD transition. Accounting for the observed analogies, we hypothesize that if extrapolated to samples larger than the microscopic ones [34], it may be possible to distinguish the sequential correlated activity resembling the pool-like dynamics.

V. SUMMARY AND DISCUSSION

With the activity in living networks exhibiting spatiotemporal organization at multiple scales [30], building a self-consistent model, both encompassing the interactions at different complexity levels and yielding a comprehensive and useful approach to neural stimuli representation and transformation, proves to be a challenging task. The mesoscopic-scale model we introduce deals with the square-lattice-based network of locally and recurrently coupled neural pools [2], whose global excitation mode consists of propagating spike packets. Such dynamic behavior, facilitated by bridging the single neuron depolarized states (sustained by synchronized input) within the connection architecture providing the synaptic strength values distributed according to the STDP learning rule, guides the formation of network spatiotemporal patterns, identified with synfire chains. Though the synfire chains in biological networks have so far been applied in recognizing invariances in a picture [67] or performing segregation in auditory (e.g., for parsing sentences into words [68]) and visual (e.g., for separating figure from the ground [69,70]) stimuli sequences, it is believed that their main field of application may lie in representing compositionality [2,70] through the hierarchical framework, comprising several transiently coupled synfire chains. Even with the role of synfire chains initially tied to information transfer, the propagation of spike packets may take place spontaneously, which makes the identification of minimal conditions (connectivity sparseness, intrinsic neuron, and synaptic parameters) for their appearance particularly important. Similar concept for networks with neurons, rather than pools as basic elements, has already been developed in detail [71].

The synfire chain development is examined by observing the neural pool clustering according to the integral activation values, calculated by applying the derived population activity Eq. (10). We find the development process to exhibit the properties of the percolation phase transition, with the pool connectedness probability p standing for the critical parameter. The conjoined effects of lattice topology, neuron refractoriness μ, and the nonzero synaptic weight value Ω are established to influence the critical probability values and universality classes which the observed phase transitions pertain to.

The regular lattice critical probabilities p_c for each of the three considered refractoriness values display monotonous decay with growing Ω, forming a family of critical lines. At the lower connectivity degree, collective effects remain weak enough within the considered Ω interval. This enables the prevalence of the leading cluster as percolation cluster, providing for monotonicity of critical probability. Further, as Ω increases, fewer number of pools is needed to form the percolation cluster, which implies a decrease in critical probabil-

ity values. At $z=8$, there exists an Ω interval where the collective effects advance the bulk cluster to become percolative, accounting for the nonmonotonicity of critical probability.

Applying the finite-size scaling method, we determined the percolation cluster fractal dimensions D for each of the lattice topologies, finding it to be considerably influenced by refractoriness value μ. At low μ, the temporal autocorrelations at single pools are significantly weakened, implying an almost complete absence of memory effects [see the third term on the right side of Eq. (10)]. This enables the emerging of feedback loops, which, at higher connectivity, cause the adjacent sites to perturb each other's respective dynamics more effectively. Such local framework at $z=8$ is expected to advance greater heterogeneity of the upcoming percolation clusters.

At moderate μ values, the temporal autocorrelation gains strength, which should be put in context with the effects of changing lattice topology. At lower connectedness degree, the temporal autocorrelation leads to trapping of local states, while, with increasing connectivity, the cross correlation between neighboring pools rises to a collective phenomenon. Thus, at $z=8$ the pool dynamics appears stationary, i.e., spike packets assume a similar form across the network. The described effects provide for the larger compactness of percolation clusters in more connected networks while keeping μ moderate.

Following the obtained $\beta/\nu_\perp$ critical exponent ratios, we posit that the phase-transition universality classes may be distinguished according to the refractoriness value. For the regular lattice topology, the DP appears as the generic universality class at nonzero refractoriness values, which is likely influenced by the lack of competition between the leading and bulk clusters. At $z=8$, the more pronounced collective effects result in the leading and bulk clusters, successively taking the role of percolation clusters as Ω increases. The generic phase transitions pertaining to PCPD universality class seem to relate to prevalence of the leading cluster, while the DIP universality class transitions correspond to the bulk cluster dominance within a limited weight interval.

From the scope of local excitation dynamics, the observed phase transitions for both lattice topologies appear to be influenced by the feedback originating recurrent activity, as some of the active pools take the role of secondary sources which reactivate the lattice sites along or near the earlier covered propagation path. For the given interaction structure, we suppose the relation between the coupling range and the average recurrent activity path to influence the critical behavior of the transitions, as corroborated by several researches conducted on grown cultures or cortical slices [34,54].

Several research groups reported critical exponents similar to ours for networks operating under a variety of different conditions. While theoretically addressing the issue of percolation phase transitions in microscopic neural networks, Kozma *et al.* [72] found DIP, DP, and PCPD universality classes corresponding to topological variations, i.e., to the absence, small and large number of the introduced distant connections, respectively. In addition, the experimental research by Breskin *et al.* [34] may have recovered the PCPD universality class in cultured networks comprised of 400–1000 neurons for both the homogeneous (excitatory neural population) and inhomogeneous (comprising mixed excitatory-inhibitory population) networks. These results possibly indicate similarity between phase transitions at microscopic and mesoscopic networks, implying that this line of research should extend to more complexly structured networks encompassing a variety of different scales. With the rich topological and dynamical conditions at all three scales, it becomes important to identify the constraints which drive the neural network phase transitions to specific universality classes.

ACKNOWLEDGMENT

This research was performed as part of the work within Project No. 141020 funded by the Serbian Ministry of Science and Technological Development.

[1] *Handbook of Brain Theory and Neural Networks*, 2nd ed., edited by M. A. Arbib (MIT, Cambridge, MA, 2003).
[2] E. Bienenstock, Network Comput. Neural Syst. **6**, 179 (1995).
[3] W. Singer, *The New Cognitive Neurosciences*, 2nd ed., edited by M. S. Gazzaniga (MIT, Cambridge, MA, 1999).
[4] D. Horn, N. Levy, and E. Ruppin, Neurocomputing **32-33**, 409 (2000).
[5] T. Tetzlaff, T. Geisel, and M. Diesmann, Neurocomputing **44-46**, 673 (2002).
[6] C. Mehring, U. Hehl, M. Kubo, M. Diesmann, and A. Aertsen, Biol. Cybern. **88**, 395 (2003).
[7] M.-O. Gewaltig, M. Diesmann, and A. Aertsen, Neural Networks **14**, 657 (2001).
[8] K. D. Harris, J. Csicsvari, H. Hirase, G. Dragoi, and G. Buzsaki, Nature (London) **424**, 552 (2003).
[9] C. Haldeman and J. M. Beggs, Phys. Rev. Lett. **94**, 058101 (2005).
[10] A. Riehle, S. Grun, M. Diesmann, and A. Aertsen, Science **278**, 1950 (1997).
[11] R. Huerta and M. Rabinovich, Phys. Rev. Lett. **93**, 238104 (2004).
[12] M. Abeles, H. Bergman, E. Margalit, and E. Vaadia, J. Neurophysiol. **70**, 1629 (1993).
[13] Y. Prut *et al.*, J. Neurophysiol. **79**, 2857 (1998).
[14] B.-Q. Mao, F. Hamzei-Sichani, D. Aronov, R. C. Froemke, and R. Yuste, Neuron **32**, 883 (2001).
[15] D. V. Buonomano, Proc. Natl. Acad. Sci. U.S.A. **100**, 4897 (2003).
[16] J.-Y. Wu, L. Guan, L. Bai, and Q. Yang, J. Neurophysiol. **86**, 2461 (2001).
[17] J. D. Rolston, D. A. Wagenaar, and S. M. Potter, J. Neurosci. **148**, 294 (2007).
[18] D. A. Wagenaar, Z. Nadasdy, and S. M. Potter, Phys. Rev. E **73**, 051907 (2006).

[19] T. Tateno, A. Kawana, and Y. Jimbo, Phys. Rev. E **65**, 051924 (2002).
[20] M. Chiappalone, M. Bove, A. Vato, M. Tedesco, and S. Martinoia, Brain Res. **1093**, 41 (2006).
[21] N. Levy, D. Horn, I. Meilijson, and E. Ruppin, Neural Networks **14**, 815 (2001).
[22] K. Kitano, H. Cateau, and T. Fukai, Neurocomputing **44-46**, 473 (2002).
[23] R. Cossart, D. Aronov, and R. Yuste, Nature (London) **423**, 283 (2003).
[24] R. Segev, I. Baruchi, E. Hulata, and E. Ben-Jacob, Phys. Rev. Lett. **92**, 118102 (2004).
[25] E. Maeda, H. P. C. Robinson, and A. Kawana, J. Neurosci. **15**, 6834 (1995).
[26] Y. Ikegaya, G. Aaron, R. Cossart, D. Aronov, I. Lampl, D. Ferster, and R. Yuste, Science **304**, 559 (2004).
[27] W. Gerstner and W. M. Kistler, *Spiking Neuron Models* (Cambridge University Press, New York, 2002).
[28] W. J. Freeman, *Mesoscopic Brain Dynamics* (Springer, London, 2000).
[29] W. J. Freeman, J. Physiol. (Paris) **94**, 303 (2000).
[30] G. Buzsaki, *Rhythms of the Brain* (Oxford University Press, New York, 2006).
[31] M. Diesmann, M.-O. Gewaltig, and A. Aertsen, Nature (London) **402**, 529 (1999).
[32] W. Maas and H. Markram, in *Microcircuits: The Interface Between Neurons and Global Brain Function*, edited by S. Grillner and A. M. Graybiel (MIT, Cambridge, MA, 2006).
[33] *The Dynamical Systems Approach to Cognition*, edited by W. Tschacher and J.-P. Dauwalder (World Scientific, Singapore, 2003), pp. 71–183.
[34] I. Breskin, J. Soriano, E. Moses, and T. Tlusty, Phys. Rev. Lett. **97**, 188102 (2006).
[35] J.-P. Eckmann, O. Feinerman, L. Gruendlinger, E. Moses, Jordi Soriano, and Tsvi Tlusty, Phys. Rep. **449**, 54 (2007).
[36] A. D. Reyes, Nat. Neurosci. **6**, 593 (2003).
[37] R. Hosaka, O. Araki, and T. Ikeguchi, Neural Comput. **20**, 415 (2008).
[38] W. M. Kistler and W. Gerstner, Neural Comput. **14**, 987 (2002).
[39] Y. Aviel and W. Gerstner, Phys. Rev. E **73**, 051908 (2006).
[40] Y. Fregnac *et al.*, in *Microcircuits: The Interface Between Neurons and Global Brain Function*, edited by S. Grillner and A. M. Graybiel (MIT, Cambridge, MA, 2006).
[41] S. Fujisawa, N. Matsuki, and Y. Ikegaya, Cereb. Cortex **16**, 639 (2006).
[42] R. Moreno-Bote and N. Parga, Phys. Rev. Lett. **94**, 088103 (2005).
[43] M. Shelley, D. McLaughlin, R. Sharpley, and J. Wielaard, J. Comput. Neurosci. **13**, 93 (2002).
[44] E. T. Lee and J. W. Wang, *Statistical Methods for Survival Data Analysis*, 3rd ed. (Wiley-Intersience, New York, 2003).
[45] D. R. Cox and V. Isham, *Point Processes* (Chapman and Hall, London, 1980).
[46] H. Haken, *Brain Dynamics* (Springer, Berlin, 2007).
[47] K. Binder, Z. Phys. B: Condens. Matter **43**, 119 (1981).
[48] K. Binder, in *Computational Methods in Field Theory*, edited by H. Gausterer and C. B. Lang (Springer-Verlag, Berlin, 1992).
[49] V. Privman, in *Finite-Size Scaling and Numerical Simulation of Statistical Systems*, edited by V. Privman (World Scientific, Singapore, 1990).
[50] P. Marcq, H. Chate, and P. Manneville, Phys. Rev. E **55**, 2606 (1997).
[51] H. Hinrichsen, Adv. Phys. **49**, 815 (2000).
[52] S. Lubeck, Int. J. Mod. Phys. B **18**, 3977 (2004).
[53] G. Odor, Rev. Mod. Phys. **76**, 663 (2004).
[54] J. M. Beggs and D. Plenz, J. Neurosci. **23**, 11167 (2003).
[55] M. A. Buice and J. D. Cowan, Phys. Rev. E **75**, 051919 (2007).
[56] H. Hinrichsen, Phys. Rev. E **63**, 036102 (2001).
[57] G. T. Barkema and E. Carlon, Phys. Rev. E **68**, 036113 (2003).
[58] G. Odor, Phys. Rev. E **62**, R3027 (2000).
[59] K. Park and I. M. Kim, Phys. Rev. E **66**, 027106 (2002).
[60] J. D. Noh and H. Park, Phys. Rev. E **69**, 016122 (2004).
[61] S. C. Park and H. Park, Phys. Rev. E **73**, 025105(R) (2006).
[62] G. Odor, Phys. Rev. E **70**, 026119 (2004).
[63] J. Kockelkoren and H. Chate, Phys. Rev. Lett. **90**, 125701 (2003).
[64] H.-K. Janssen, F. van Wijland, O. Deloubriere, and U. C. Tauber, Phys. Rev. E **70**, 056114 (2004).
[65] I. Dornic, H. Chate, and M. Munoz, e-print arXiv:cond-mat/0505171.
[66] R. Dickman and Marcio Argollo Ferreira de Menezes, Phys. Rev. E **66**, 045101(R) (2002).
[67] H. M. Arnoldi, R. K. Englemeier, and W. Brauer, Biol. Cybern. **80**, 433 (1999).
[68] C. Jacquemin, SIGART Bulletin **5**, 12 (1994).
[69] M. Abeles, G. Hayon, and D. Lehmann, J. Comput. Neurosci. **17**, 179 (2004).
[70] G. Hayon, M. Abeles, and D. Lehmann, J. Comput. Neurosci. **18**, 41 (2005).
[71] T. Nowotny and R. Huerta, Biol. Cybern. **89**, 237 (2003).
[72] R. Kozma, M. Puljic, P. Balister, B. Bollobas, and W. J. Freeman, Biol. Cybern. **92**, 367 (2005).